JCTC Journal of Chemical Theory and Computation

Electronic Structure and Reactivity of Boron Nitride Nanoribbons with Stone-Wales Defects

Wei Chen,[†] Yafei Li,[‡] Guangtao Yu,[§] Zhen Zhou,*[‡] and Zhongfang Chen*[†]

Department of Chemistry, Institute for Functional Nanomaterials, University of Puerto Rico, Rio Piedras Campus, San Juan, Puerto Rico 00931, Institute of New Energy Material Chemistry, Institute of Scientific Computing, Nankai University, Tianjin 300071, P. R. China, and The State Key Laboratory of Theoretical and Computational Chemistry, Institute of Theoretical Chemistry, Jilin University, Changchun 130023, P.R. China

Abstract: Gradient-corrected density functional theory (DFT) computations were performed to investigate the geometry, electronic property, formation energy, and reactivity of Stone−Wales (SW) defects in zigzag-edge and armchair-edge boron nitride nanoribbons (BNNRs). The formation energies of SW defects increase with an increase in the widths of BNNRs and are orientation-dependent. SW defects considerably reduce the band gaps of BNNRs independent of the defect orientations. In addition, the local chemical reactivity of SW defects and edge sites in zigzag-edge and armchair-edge BNNRs was probed with the CH_2 cycloaddition reaction. Independent of the nanoribbon types and the SW defect orientations, the reactions at SW defect sites are more exothermic than those at the center of perfect BNNRs, and the newly formed B−B and N−N bonds are the most reactive sites, followed by the 5−7 ring fusions.

1. Introduction

Since its experimental discovery in 2004,[1,2] graphene, a single atomic layer of graphite, has brought us a new revolution in materials science due to its many charming, unusual properties.[3−6] For example, graphene is the strongest material ever measured,[3] chemically stable and inert, and conducts electricity better than any other known material at room temperature.[5] These outstanding mechanical, chemical, and electronic properties have stimulated great interest and extensive experimental and theoretical research on the graphene-based materials family.[7−31] As one important member of this family, graphene nanoribbons (GNRs), a new type of one-dimensional (1-D) graphene-based material, have been synthesized by cutting the two-dimensional graphene.[1] The electronic and magnetic properties of GNRs have been widely studied.[15−31] The tight-binding computational results showed that, depending upon the width and orientation of the edges, the H-terminated GNRs can be semiconducting or metallic.[16−18] While more reliable first-principles calculations revealed a nonzero band gap for GNRs independent of the width and orientation of the edges.[19,24,25] In particular, this theoretical prediction was confirmed by the recent experiments.[27,28] Moreover, the zigzag GNRs are magnetic,[22,24] and applying electric field[29] or edge-modifications[30,31] renders them half-metallic.

Inspired by the intensive studies on GNRs, researchers have also broadened the field to inorganic nanoribbons, such as BN,[32] BNC,[33] B,[34] BC_3,[35] B_2C,[36] SiC,[37] ZnO,[38] and MoS_2[39] nanoribbons. Among them, as an analogy to GNRs structurally, BN nanoribbons (BNNRs) have attracted more attention.[32,40−47] Note that single-layer and few-atomic-layer hexagonal BN sheets have been experimentally realized.[48−52] In particular, Meyer et al.[51] synthesized the clean single-layer hexagonal boron nitride graphene and reported atomic resolution imaging. Zhi et al.[52] achieved large-scale fabrication of boron nitride nanosheets (as thin as three layers), and these inorganic sheets were utilized to improve thermal and mechanical properties of the polymeric composites.

* Corresponding author e-mail: zhouzhen@nankai.edu.cn (Z.Z.); zhongfangchen@gmail.com (Z.C.).

[†] University of Puerto Rico.

[‡] Nankai University.

[§] Jilin University.

Therefore, similar to the case of GNRs, it is highly possible that the BNNRs may be synthesized by cutting single-layer hexagonal BN. Due to the large ionicity of BN, BNNRs may possess novel properties different from those of GNRs. Theoretically, perfect BNNRs have been predicted to present semiconductor behavior, regardless of their width and orientation of the edges.[40] The H-terminated BNNRs are nonmagnetic,[40] while the bare zigzag BNNRs are magnetic.[32,46] An applied transverse electric field can induce electron reorganization and control the band gap of bare zigzag BNNRs to produce a metallic−semiconducting−half-metallic transition.[32] The half-metallicity is also found in BNNRs with only the B edge passivated with hydrogen.[46,47] These open promising opportunities for the application of BNNRs in electro-optical devices.

Perfect nanomaterials exhibit attractive physical and chemical properties; however, defects are inevitable in reality, such as vacancies, adatoms, and topological defects, which may impact significantly the electronic properties and chemical reactivity of nanomaterials.[53−66] A well-known example is the Stone−Wales (SW) defect, which is comprised of two pairs of five-membered and seven-membered rings (5−7−7−5) formed by rotating one bond of the traditional six-membered ring by 90°.[67] The effect of SW defects on the electronic and mechanical properties of carbon nanotubes (CNTs), BN nanotubes (BNNTs), and GNRs has drawn considerable attention, especially in terms of chemical reactivity.[55,56,61,62,64−66] All of these studies show that the SW defects play an important role in the structural reconstruction, electronic properties, and chemical reactivity of nanomaterials. To the best of our knowledge, however, no investigations have been performed on the electronic properties and chemical reactivity of BNNRs with SW defects.

In this study, we carried out systematic first-principles computations to investigate the formation energies and electronic properties of zigzag and armchair BNNRs with SW defects. Because of the stronger reactivity, carbene (CH_2) is used as a probe to examine the chemical reactivity of SW defect sites in BNNRs with different edges. In particular, we focus on the effects of the SW defects and defect orientation on the formation energies, band structures, and chemical reactivity of these BNNRs.

2. Computational Methods

The generalized gradient approximation with the PW91 functional[68] and a 360 eV cutoff for the plane-wave basis set were employed for all of the DFT computations with the Vienna *ab initio* simulation package (VASP).[69−72] The ultrasoft pseudopotentials[73] were used to model the electron−ion interactions. Interactions between SW defects and their images were avoided in our computational supercell models, for which the distance between two SW defects is longer than 10 Å in both zigzag BNNRs (zBNNRs) and armchair BNNRs (aBNNRs). The edges of BNNRs are terminated by hydrogen atoms to remove dangling bonds. Five k points were used for sampling the 1-D Brillouin zone, and the convergence threshold was set as 10^{-4} eV in energy and 10^{-3} eV/Å in force. The positions of all of the atoms in the supercell were fully relaxed during the geometry optimiza-
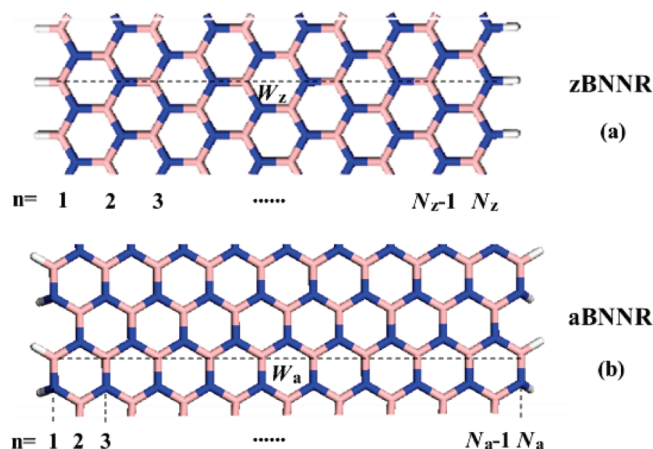

Figure 1. Geometric structure for H-terminated BN nanoribbons: (a) zigzag-edged and (b) armchair-edged. The blue, pink, and white colors represent N, B, and H atoms, respectively.

tions. On the basis of the equilibrium structures, 21 k points were used to compute band structures.

Defect formation energies (energies required to form SW defects) are defined as

$$E_F = E_{SW} - E_{perfect} \qquad (1)$$

where E_{SW} and $E_{perfect}$ are the total energy of the BNNR containing a SW defect and that of the perfect BNNR, respectively. Note that this definition does not take into account the energy barrier height for the formation of the SW defect, which may be higher than the calculated formation energy on the basis of the ground state energy differences. The reaction energy for the cycloaddition of CH_2 group is estimated as

$$E_R = E_{total} - E_{BNNR} - E_{CH_2} \qquad (2)$$

where E_{total}, E_{BNNR}, and E_{CH_2} are the total energy of the CH_2-added BNNR, the pristine BNNR, and the CH_2 group, respectively.

3. Results and Discussion

3.1. Geometric Structures of SW Defects in zBNNRs and aBNNRs. By convention, as shown in Figure 1, the structures of zBNNRs and aBNNRs are classified by the number of zigzag chains N_z and dimer lines N_a across the ribbon width, respectively. Figure 2 represents the perfect and defective structures of 8-zBNNR and 11-aBNNR. There are two kinds of B−N bonds in zBNNRs and aBNNRs. One is parallel or perpendicular to the axis, and the other is slanted. These are denoted by bond "1" and bond "2" in Figure 2a and d, respectively. Consequently, two types of SW defects for each of the BNNRs (labeled as SW-1 and SW-2) are possible via rotating bonds 1 or 2 by 90°, and new B−B and N−N bonds appear in all of the defective BNNRs. These new B−B and N−N bonds in 8-zBNNR with SW-1 (1.663 and 1.433 Å) are slightly shorter than those in 8-zBNNR with SW-2 (1.664 and 1.439 Å), while the corresponding B−B and N−N bonds in 11-aBNNR with SW-1 (1.672 and 1.443 Å) are somewhat longer than those
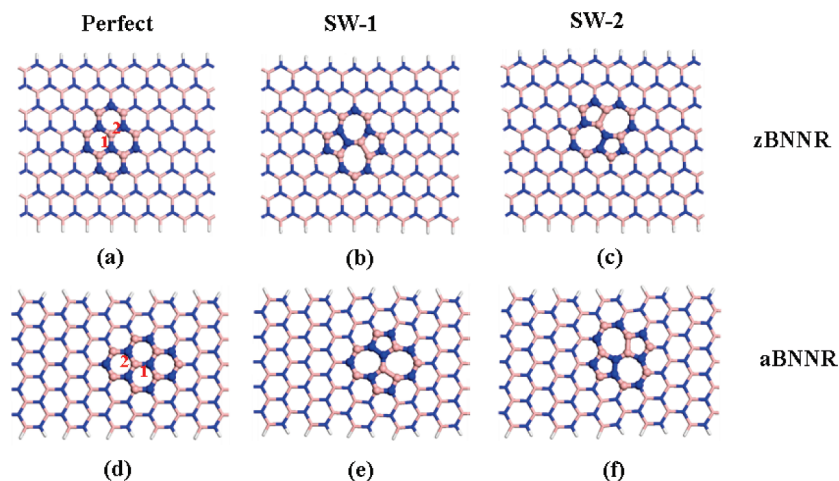
Figure 2. Optimized structures of BNNRs: (a, d) perfect and (b/e, c/f) with various SW defects.

Table 1. Bond Lengths, Pyramidalization Angles, and Formation Energies Related to SW Defects in 8-zBNNRs and 11-aBNNRs

| species | | d_{B-N} (Å) | d_{B-B} (Å) | d_{N-N} (Å) | Θ_p (degree) | | E_F (eV) |
					B^a	N^b	
zBNNRs	perfect	1.446^c					
		1.443^d					
	SW-1	1.353^e	1.663	1.433	0.15	0.18	6.50
	SW-2	1.363^e	1.664	1.439	0.75	1.60	6.31
aBNNRs	perfect	1.448^c					
		1.446^d					
	SW-1	1.365^e	1.672	1.443	0.54	0.15	6.30
	SW-2	1.367^e	1.668	1.435	0.18	0.62	5.96

^{a} The B atom at the 7−7 ring fusions of SW defects. ^{b} The N atom at the 7−7 ring fusions of SW defects. ^{c} Bond 1. ^{d} Bond 2 (see Figure 2a and d). ^{e} The B−N bonds at the 7−7 ring fusions of SW defects.

in 11-aBNNR with SW-2 (1.668 and 1.435 Å, respectively). Moreover, the B−N bonds at the 7−7 ring fusions of SW defects in all defective BNNRs are shorter than those in perfect BNNRs. For the defective BNNRs, most of the bonds are slightly longer than the corresponding bonds in BNNTs with SW defects due to local curvatures of BNNTs.[65]

Usually, the pyramidalization angle ($\Theta_p = \theta_{\sigma\pi} - 90°$) is used to measure the degree of sp^3 hybridization of an atom, where $\theta_{\sigma\pi}$ is the angle between σ and π bonds.[74−76] Note that perfect BNNRs have no pyramidalization angle because of their π-conjugated planar structures. However, the Θ_p angle can describe the degree of sp^3 hybridization for the B and N atoms at the 7−7 ring fusions of SW defects, where the B and N atoms are slightly outward from the plane due to the formation of SW defects (Table 1). Obviously, these Θ_p angles may reflect the structural deformation owing to the defect formation. As shown in Table 1, the respective Θ_p angles of the B and N atoms at the SW-1 site are 0.15 and 0.18° for zBNNRs and 0.54 and 0.15° for aBNNRs, while the corresponding values at the SW-2 site are 0.75 and 1.60° for zBNNRs and 0.18 and 0.62° for aBNNRs, respectively. Clearly, the orientation of SW defects in BNNRs has different effects on the Θ_p angles: independent of the orientation of the edges in BNNRs, the deviations of the B and N atoms at the 7−7 ring fusions of SW-1 sites are less than those of SW-2 sites. Note that deviations can
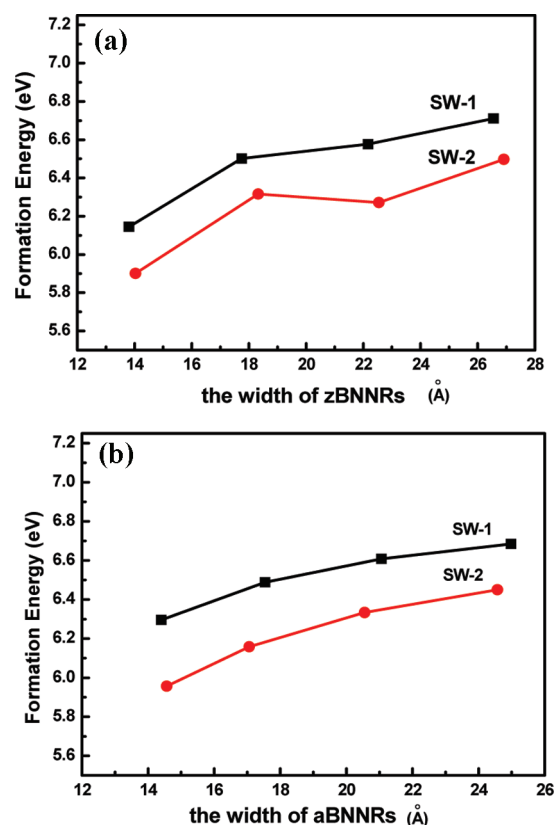

Figure 3. Formation energies of SW defects as a function of the widths of BNNRs: (a) zBNNRs and (b) aBNNRs.

be directly reflected by Θ_p angles in BNNRs. These tiny deviations of the B and N atoms at the 7−7 ring fusions of SW defects may influence the formation energies of SW defects in BNNRs. As shown in Table 1, in contrast to the BNNRs with SW-1, the more deformed BNNRs with SW-2 are more favorable energetically and possess smaller defect formation energy, independent of the orientation of the edges.

3.2. Formation Energies of SW Defects in zBNNRs and aBNNRs with Different Widths. The formation energies of SW defects in CNTs[77,78] and BNNTs[65] have been reported, which depend not only on the defect orientations but also on the tube radii. It has been pointed out that SW defects form with more difficulty in larger-diameter BNNTs
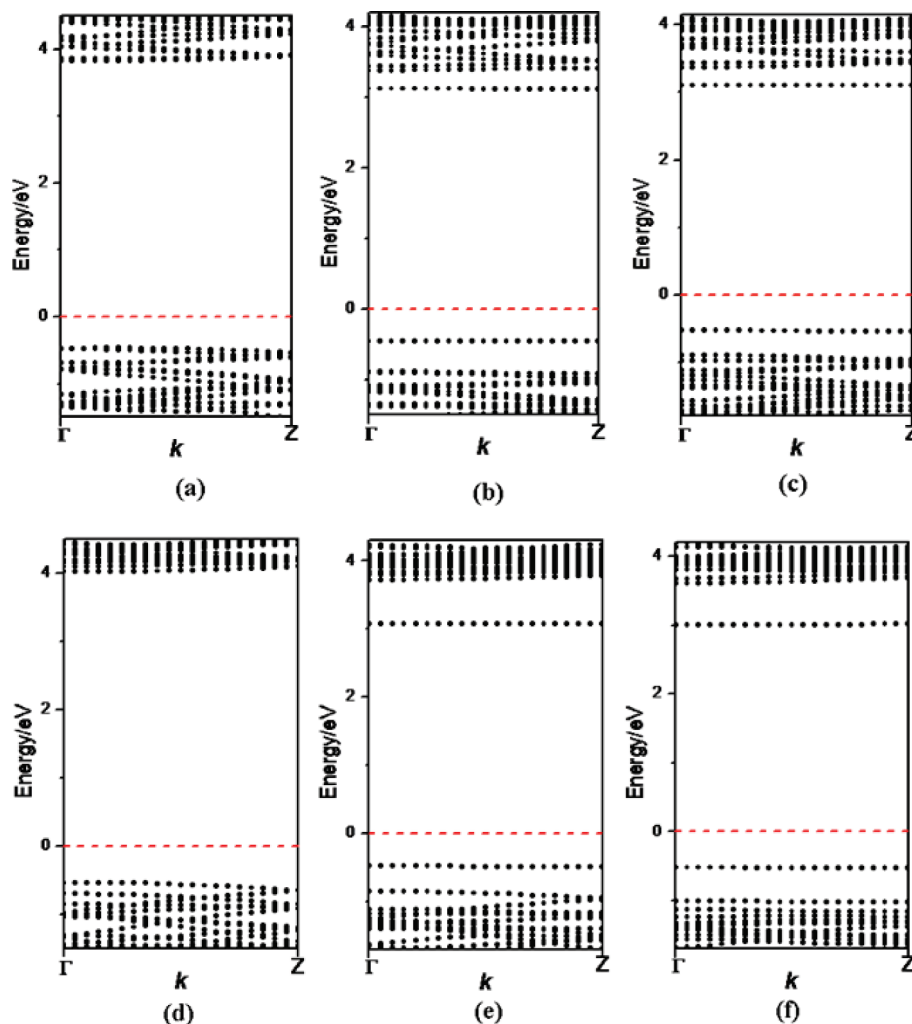
Figure 4. Band structures of 8-zBNNRs—perfect (a), with SW-1 (b), and with SW-2 (c)—11-aBNNRs: perfect (d), with SW-1 (e), and with SW-2 (f).

and CNTs.[65,78] Also, in the BN graphene sheet, the formation energy of SW defects is up to 7.28 eV.[65] Naturally, it can be expected that forming SW defects in BNNRs will be more difficult than in BNNTs,[65] which is supported by our present computations.

We computed the formation energies of SW defects in zBNNRs and aBNNRs as a function of the ribbon width (Figure 3), for which both kinds of SW defects (SW-1 and SW-2) in a series of zBNNRs and aBNNRs with various widths (N_z = 6, 8, 10, 12 and N_a = 11, 13, 16, 19) were considered. Our computations show that the formation energies of both SW-1 and SW-2 increase with increasing widths of zBNNRs and aBNNRs (Figure 3). The narrowest ribbons have the lowest formation energies of SW defects, which are 6.14 eV for SW-1 in 6-zBNNR, 5.90 eV for SW-2 in 6-zBNNR, 6.30 eV for SW-1 in 11-aBNNR, and 5.96 eV for SW-2 in 11-aBNNR. When their widths are the same, the formation energies of SW-1 are always larger than those of SW-2 in all of the zBNNRs and aBNNRs. Obviously, the orientation of the SW defect has different effects on the formation energies of both zBNNRs and aBNNRs. The SW-2 defect is closer to the edges than SW-1 defect in both types of BNNRs (Figure 2). Consequently, the SW-2 defect is easier to form than the SW-1 defect due to the easier

deformation of the edge, and the more deformed BNNRs with SW-2 defect possess a smaller formation energy, as shown in Table 1.

3.3. Band Structures of zBNNRs and aBNNRs with SW Defects. Similar to BNNTs,[65] the electronic band structures of perfect and defective zBNNRs and aBNNRs show typical semiconductor behavior (Figure 4). The perfect BNNRs display a 4.56 eV direct band gap for 11-aBNNR and a 4.28 eV indirect band gap for 8-zBNNR (Figure 4a and d), which are reasonably consistent with the results reported by Du et al.[40]

Previous theoretical studies pointed out that the electronic band structures of BNNTs can only be modified slightly at the presence of some defects.[57-59,65] However, different from the BNNTs with SW defects,[65] the formation of SW defects in BNNRs has significant effects on their electronic band structures, although all of the BNNRs with SW defects still retain typical wide-band-gap semiconductor character. As shown in Figure 4, introducing SW defects in perfect BNNRs leads to new levels of the top valence band and the bottom conduction band. Consequently, the band gaps of BNNRs with SW defects are reduced significantly, by 0.71, 0.65, 1.00, and 1.03 eV, respectively, for 8-zBNNR with SW-1, 8-zBNNR with SW-2, 11-aBNNR with SW-1, and 11-
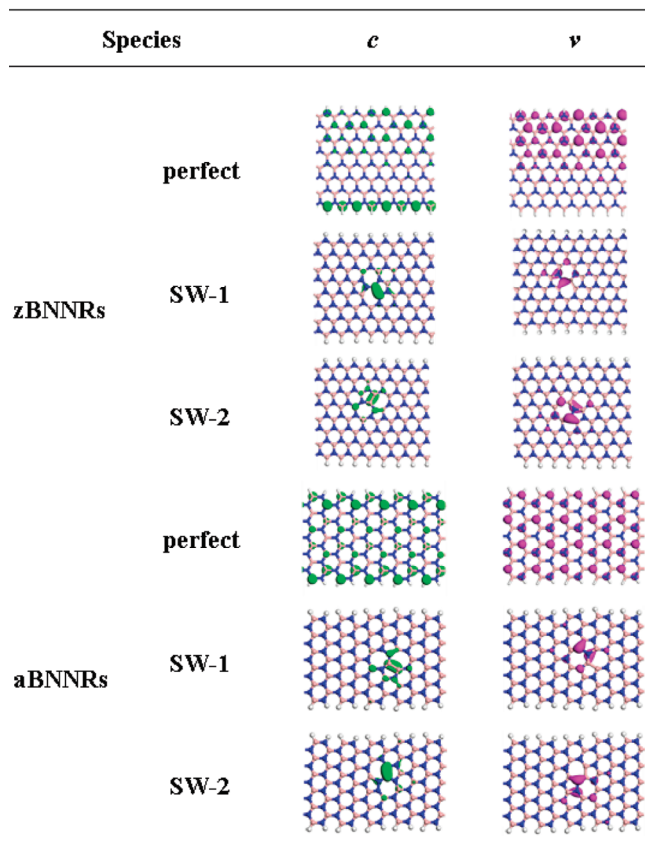
Figure 5. Electron density isosurfaces of the highest-energy valence (*v*) and the lowest-energy conduction (*c*) bands of perfect and defective zBNNRs and aBNNRs.

aBNNR with the SW-2 defect. The orientation of SW defects has almost no effect on the band gap reduction of zBNNRs and aBNNRs.

To clearly examine the character of these new levels in defective BNNRs, we plotted the electron density isosurfaces of the valence bands and conduction bands of perfect and defective BNNRs (Figure 5). For the perfect zBNNR, its top valence band is mainly from N atoms close to and on the N edge, while its bottom conduction band is mainly from the B atoms of the B edge; in contrast, for perfect aBNNR, the top valence band and bottom conduction band originate from almost all of the N atoms and all of the B atoms, respectively. Obviously, the edge orientation of perfect BNNRs affects the composition of their top valence bands and bottom conduction bands. In comparison with perfect BNNRs, for all of the defective BNNRs, independent of the edge and defect orientation, the top valence bands originate mainly from the N atoms in the N−N bonds at the SW defects sites, while the bottom conduction bands are mainly from the B atoms in the B−B bonds at the SW defects sites. Obviously, the reduction of the band gap of BNNRs with SW defects is due to the localized defect states appearing within the gap of the pristine BNNRs, instead of the shifting of the original valence and conductance bands. This is similar to the case of the BNNTs with SW defects reported by Li et al.[65] However, compared with the defective BNNTs, BNNRs with SW defects show a much larger reduction of band gaps, which indicates that the newly formed N−N bonds and B−B

bonds of SW defect sites are more unfavorable due to the planar structures of BNNRs.

Additionally, the introduction of SW defects obviously reduces the band gaps of defective BNNRs, which implies that the band gap of BNNRs is not so robust. As a result, it is reasonable for us to suppose that the band gap of BNNRs may be further reduced, even close to having metal behavior, such as by chemical modification. These interesting electronic properties will make BNNRs promising materials for many potential applications, particularly in nanoelectronics.

3.4. Chemical Reactivity of SW Defects in zBNNRs and aBNNRs. Defects sites are usually considered as the center of chemical reactions in nanomaterials. The chemical reactivities of SW defects in CNTs and BNNTs have been widely investigated,[61,62,64,65,79,80] in which some small species such as CH_2, O, O_3, and CO are deemed to be excellent adsorbates due to their high reactivity. A previous theoretical study, reported by Lu et al., indicated that the central C−C bond of the SW-defect site in CNTs is less reactive than all of the other sites.[61] However, An et al. found that the SW defects in BNNTs are more reactive than the perfect sites.[64] These different chemical reactivities are related to the local deformation, characterized with the pyramidalization angles Θ_p of the involved atoms. The increased Θ_p angle has a significant contribution to high chemical reactivities.

In this work, carbene cycloadditions were used to probe the chemical reactivity of SW defect sites in zBNNRs and aBNNRs. Some characteristic sites related to SW defects were considered, as well as two sites on the edges of perfect and defective BNNRs, because the edge plays an important role in nanoribbons.[26,27] All of the addition sites on the perfect and defective BNNRs with the different edges are illustrated in Figure 6. Some typical structures of CH_2 cycloaddition to perfect BNNRs and the B−B, N−N, and 7−7 ring fusion sites in defective BNNRs are shown in Figure S1 (Supporting Information). Our calculated reaction energies in Tables 2 and 3 reveal that these CH_2 cycloadditions are favorable thermodynamically. The chemical reactivities of the B−N bonds on edges are higher than those in the center for perfect BNNRs. In defective BNNRs, the chemical reactivities of the bonds related to SW defects are comparable to or even higher than those of the bonds on the edges due to the existence of tiny pyramidalization angles for the related atoms in SW defect sites. In particular, the newly formed B−B and N−N bonds are the most reactive sites in defective BNNRs due to their energetically unfavorable character. Among all of the sites including 7−7, 6−7, 5−7, and 5−6 ring fusions, the chemical reactivity of 5−7 ring fusion sites (sites 4 and 5) are higher than those of other sites, followed by 6−7 ring fusion sites. All of the above results are independent of the type of BNNRs.

4. Conclusion

SW defects in a series of zBNNRs and aBNNRs were investigated by means of DFT computations. By rotating different B−N bonds, two kinds of SW defects (named SW-1 and SW-2) for zBNNRs and aBNNRs were considered. The formation of the SW defects in all BNNRs changes the local
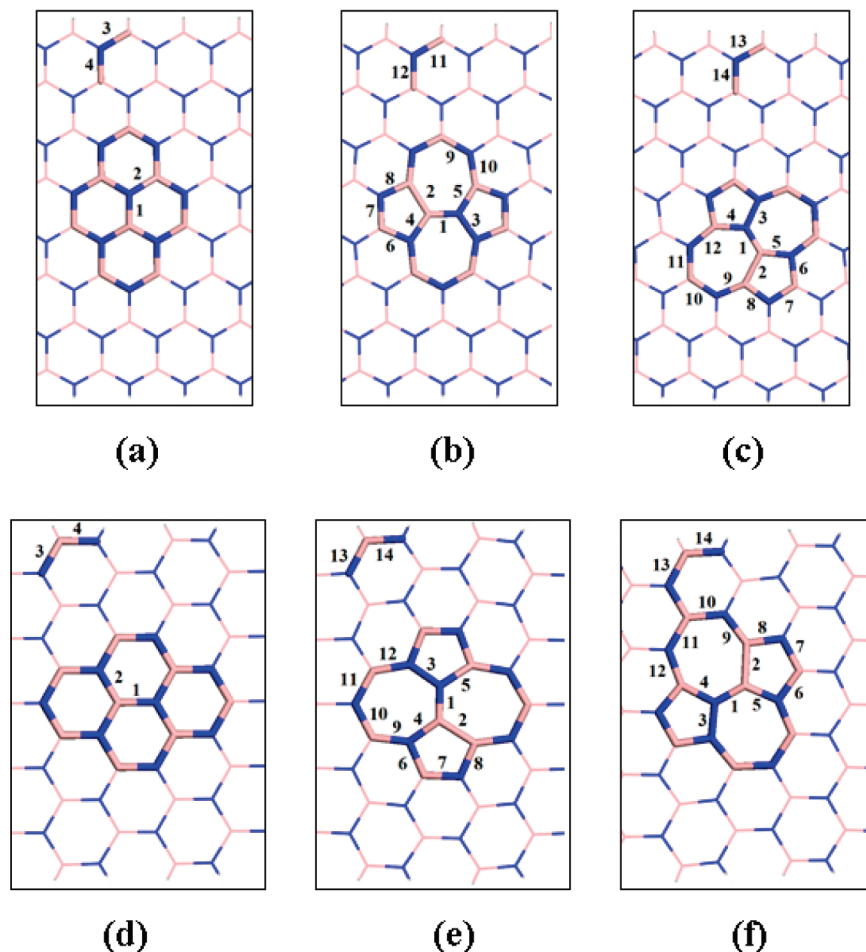
Figure 6. Possible sites for cycloadditions of CH_2 to perfect and defective BNNRs: (a–c) for zBNNRs and (d–f) for aBNNRs.

Table 2. CH_2 Cycloaddition Reaction Energies (eV) on Corresponding Sites (Figure 6a–c) in the Perfect and Defective 8-zBNNRs

reaction sites	perfect	SW-1	SW-2
1	−1.60	−2.27	−2.22
2	−1.62	−4.62	−4.54
3	−2.33	−4.81	−4.64
4	−2.02	−2.93	−3.13
5		−3.13	−2.79
6		−2.07	−2.12
7		−2.36	−2.20
8		−2.42	−2.46
9		−2.53	−2.24
10		−3.03	−2.27
11		−2.08	−2.49
12		−2.06	−2.89
13			−2.43
14			−2.06

Table 3. CH_2 Cycloaddition Reaction Energies on Corresponding Sites (Figure 6d–f) in the Perfect and Defective 11-aBNNRs

reaction sites	perfect	SW-1	SW-2
1	−1.62	−2.22	−2.09
2	−1.62	−4.45	−4.38
3	−2.45	−4.69	−4.51
4	−2.36	−2.77	−2.89
5		−3.08	−2.63
6		−2.12	−1.97
7		−2.16	−2.14
8		−2.40	−2.33
9		−2.02	−2.07
10		−2.13	−2.52
11		−2.40	−2.52
12		−2.58	−2.82
13		−2.47	−1.97
14		−2.42	−2.34

curvature at defect sites and results in small pyramidalization angles of the related atoms. Compared with BNNTs, BNNRs show larger formation energies of SW defects due to their planar structures. The SW orientations have an impact on their formation energies, and SW-2 defects are preferred energetically over SW-1 defects in BNNRs, independent of the edge orientation. The chemical reactivity of SW defects in BNNRs was investigated by using the CH_2 cycloaddition reactions. All of the CH_2 cycloadditions in perfect and defective BNNRs are exothermic and favorable thermodynamically.

namically. The reactions at SW defects sites are more exothermic than those in the center of perfect BNNRs. The newly formed B−B and N−N bonds are the most reactive sites, followed by the 5−7 ring fusions, irrespective of the types of ribbon edges. Moreover, independent of the SW defect orientation, the formation of SW defects significantly narrows the energy gaps of the defective BNNRs, though they still retain typical wide-band-gap semiconductor behavior. It is indicated that the band gap of BNNRs is not so robust, and it is highly possible to further reduce their

band gap by chemical modification. These findings are useful to design new nanodevices on the basis of BNNRs.

Supporting Information Available: The structures of the CH_2 cycloaddition at some characteristic sites of perfect and defective BNNRs. This material is available free of charge via the Internet at http://pubs.acs.org.

References

(1) Novoselov, K. S.; Geim, A. K.; Morozov, S. V.; Jiang, D.; Zhang, Y.; Dubonos, S. V.; Grigoreva, I. V.; Firsov, A. A. *Science* **2004**, *306*, 666–669.

(2) Novoselov, K. S.; Jiang, D.; Schedin, F.; Booth, T. J.; Khotkevich, V. V.; Morozov, S. V.; Geim, A. K. *Proc. Natl. Acad. Sci. U. S. A.* **2005**, *102*, 10451–10453.

(3) Lee, G.; Wei, X.; Kysar, J. W.; Hone, J. *Science* **2008**, *321*, 385–388.

(4) Zhang, Y.; Tan, Y.-W.; Stormer, H. L.; Kim, P. *Nature* **2005**, *438*, 201–204.

(5) Ponomarenko, L. A.; Schedin, F.; Katsnelson, M. I.; Yang, R.; Hill, E. W.; Novoselov, K. S.; Geim, A. K. *Science* **2008**, *320*, 356–358.

(6) Kan, E. J.; Li, Z. Y.; Yang, J. L. *Nano* **2008**, *3*, 433–442.

(7) Elias, D. C.; Nair, R. R.; Mohiuddin, T. M. G.; Morozov, S. V.; Blake, P.; Halsall, M. P.; Ferrairi, A. C.; Boukhvalov, D. W.; Katsnelson, M. I.; Geim, A. K. *Science* **2009**, *323*, 610–613.

(8) Berger, C.; Song, Z.; Li, X.; Wu, X.; Brown, N.; Naud, C.; Mayou, D.; Li, T.; Hass, J.; Marchenkov, A. N.; Conrad, E. H.; First, P. N.; Heer, W. A. D. *Science* **2006**, *312*, 1191–1196.

(9) Ci, L.; Xu, Z.; Wang, L.; Gao, W.; Ding, F.; Kelly, K.; Yakobson, B. I.; Ajayan, P. *Nano Res.* **2008**, *1*, 116–122.

(10) Chen, Z.; Lin, Y.; Rooks, M. J.; Avouris, P. *Physica E* **2007**, *40*, 228–232.

(11) Singh, A. K.; Yakobson, B. I. *Nano Lett.* **2009**, *9*, 1540–1543.

(12) Boukhvalov, D. W.; Katsnelson, M. I.; Lichtenstein, A. I. *Phys. Rev. B* **2008**, *77*, 035427.

(13) Li, Y.; Zhou, Z.; Shen, P.; Chen, Z. *J. Phys. Chem. C* **2009**, *113*, 15043–15045.

(14) Li, Y.; Zhou, Z.; Shen, P.; Chen, Z. *ACS Nano* **2009**, *3*, 1952–1958.

(15) Ezawa, M. *Phys. Rev. B* **2006**, *73*, 045432.

(16) Fujita, M.; Wakabayashi, K.; Nakada, K.; Kusakabe, K. *J. Phys. Soc. Jpn.* **1996**, *65*, 1920–1923.

(17) Wakabayashi, K.; Fujita, M.; Ajiki, H.; Sigrist, M. *Phys. Rev. B* **1999**, *59*, 8271–8282.

(18) Nakada, K.; Fujita, M.; Dresselhaus, G.; Dresselhaus, M. S. *Phys. Rev. B* **1996**, *54*, 17954–17961.

(19) Son, Y.; Cohen, M.; Louie, S. *Phys. Rev. Lett.* **2006**, *97*, 216803.

(20) Ezawa, M. *Physica E* **2008**, *40*, 1421–1423.

(21) Ezawa, M. *Phys. Rev. B* **2007**, *76*, 245415.

(22) Kudin, K. N. *ACS Nano* **2008**, *2*, 516–522.

(23) Wassman, T.; Seitsonen, A. P.; Saitta, A. M.; Lazzeri, M.; Mauri, F. *Phys. Rev. Lett.* **2008**, *101*, 096402.

(24) Barone, V.; Hod, O.; Scuseria, G. E. *Nano Lett.* **2006**, *6*, 2748–2754.

(25) Jiang, D. E.; Sumpter, B. G.; Dai, S. *J. Chem. Phys.* **2007**, *127*, 124703.

(26) Jiang, D. E.; Sumpter, B. G.; Dai, S. *J. Chem. Phys.* **2007**, *126*, 134701.

(27) Ritter, K. A.; Lyding, J. W. *Nat. Mater.* **2009**, *8*, 235–242.

(28) Li, X. L.; Wang, X. R.; Zhang, L.; Lee, S. W.; Dai, H. J. *Science* **2008**, *319*, 1229–1232.

(29) Son, Y. W.; Cohen, M. L.; Louie, S. G. *Nature (London)* **2006**, *444*, 347–349.

(30) Hod, O.; Barone, V.; Peralta, J. E.; Scuseria, G. E. *Nano Lett.* **2007**, *7*, 2295–2299.

(31) Kan, E. J.; Li, Z. Y.; Yang, J. L.; Hou, J. G. *J. Am. Chem. Soc.* **2008**, *130*, 4224–4225.

(32) Barone, V.; Peralta, J. E. *Nano Lett.* **2008**, *8*, 2210–2214.

(33) Nakamura, J.; Nitta, T.; Natori, A. *Phys. Rev. B* **2005**, *72*, 205429.

(34) Ding, Y.; Yang, X.; Ni, J. *Appl. Phys. Lett.* **2008**, *93*, 043107.

(35) Ding, Y.; Wang, Y. L.; Ni, J. *Appl. Phys. Lett.* **2009**, *94*, 073111.

(36) Wu, X.; Pei, Y.; Zeng, X. C. *Nano Lett.* **2009**, *9*, 1577–1582.

(37) Sun, L.; Li, Y.; Li, Z.; Li, Q.; Zhou, Z.; Chen, Z.; Yang, J.; Hou, J. G. *J. Chem. Phys.* **2008**, *129*, 174114.

(38) Botello-Méndez, A. R.; López-Urías, F.; Terrones, M.; Terrones, H. *Nano Lett.* **2008**, *8*, 1562–1565.

(39) Li, Y.; Zhou, Z.; Zhang, S.; Chen, Z. *J. Am. Chem. Soc.* **2008**, *130*, 16739–16744.

(40) Du, A.; Smith, S. C.; Lu, G. *Chem. Phys. Lett.* **2007**, *447*, 181–186.

(41) Zhang, Z.; Guo, W. *Phys. Rev. B* **2008**, *77*, 075403.

(42) Park, C. H.; Louie, S. G. *Nano Lett.* **2008**, *8*, 2200–2203.

(43) Jin, C.; Lin, F.; Suenaga, K.; Iijima, S. *Phys. Rev. Lett.* **2009**, *102*, 195505.

(44) Wu, X.; Wu, M.; Zeng, X. C. *Front. Phys. China* **2009**, *4* (3), 367–372.

(45) Ding, Y.; Wang, Y. L.; Ni, J. *Appl. Phys. Lett.* **2009**, *94*, 233107.

(46) Lai, L.; Lu, J.; Wang, L.; Luo, G.; Zhou, J.; Qin, R.; Gao, Z.; Mei, W. N. *J. Phys. Chem. C* **2009**, *113*, 2273–2276.

(47) Zheng, F.; Zhou, G.; Liu, Z.; Wu, J.; Duan, W.; Gu, B.; Zhang, S. B. *Phys. Rev. B* **2008**, *78*, 205415.

(48) Nagashima, A.; Tejima, N.; Gamou, Y.; Kawai, T.; Oshima, C. *Phys. Rev. Lett.* **1995**, *75*, 3918–3921.

(49) Pacilé, D.; Meyer, J. C.; Girit, C.; Zettl, A. *Appl. Phys. Lett.* **2008**, *92*, 133107.

(50) Han, W.-Q.; Wu, L.; Zhu, Y.; Watanabe, K.; Taniguchi, T. *Appl. Phys. Lett.* **2008**, *93*, 223103.

(51) Meyer, J. C.; Chuvilin, A.; Algara-Siller, G.; Biskupek, J.; Kaiser, U. *Nano Lett.* **2009**, *9*, 2683–2689.

(52) Zhi, C.; Bando, Y.; Tang, C.; Kuwahara, H.; Golberg, D. *Adv. Mater.* **2009**, *21*, 2889–2893.

(53) Wei, D.; Liu, Y.; Wang, Y.; Zhong, H.; Huang, L.; Yu, G. *Nano Lett.* **2009**, *9*, 1752–1758.

(54) Chandra, N.; Namilae, S.; Shet, C. *Phys. Rev. B* **2004**, *69*, 094101.

(55) Wang, C. C.; Zhou, G.; Liu, H. T.; Wu, J.; Qiu, Y.; Gu, B. L.; Duan, W. H. *J. Phys. Chem. B* **2006**, *110*, 10266–10271.

(56) Chakrapani, N.; Zhang, Y. M.; Nayak, S. K.; Moore, J. A.; Carroll, D. L.; Choi, Y. Y.; Ajayan, P. M. *J. Phys. Chem. B* **2003**, *107*, 9308–9311.

(57) Piquini, P.; Baierle, R. J.; Schmidt, T. M.; Fazzio, A. *Nanotechnology* **2005**, *16*, 827–831.

(58) Schmidt, T. M.; Baierle, R. J.; Piquini, P.; Fazzio, A. *Phys. Rev. B* **2003**, *67*, 113407.

(59) Zobelli, A.; Ewels, C. P.; Gloter, A.; Seifert, G.; Stephan, O.; Csillag, S.; Colliex, C. *Nano Lett.* **2006**, *6*, 1955–1960.

(60) Ren, Y.; Xiao, T.; Liao, K. *Phys. Rev. B* **2006**, *74*, 045410.

(61) Lu, X.; Chen, Z.; Schleyer, P. v. R. *J. Am. Chem. Soc.* **2005**, *127*, 20–21.

(62) Bettinger, H. F. *J. Phys. Chem. B* **2005**, *109*, 6922–6924.

(63) Dinadayalane, T. C.; Leszczynski, J. *Chem. Phys. Lett.* **2007**, *434*, 86–91.

(64) An, W.; Wu, X.; Yang, J. L.; Zeng, X. C. *J. Phys. Chem. C* **2007**, *111*, 14105–14112.

(65) Li, Y. F.; Zhou, Z.; Golberg, D.; Bando, Y.; Schleyer, P. v. R.; Chen, Z. F. *J. Phys. Chem. C* **2008**, *112*, 1365–1370.

(66) Boukhvalov, D. W.; Katsnelson, M. I. *Nano. Lett.* **2008**, *8*, 4373–4379.

(67) Stone, A. J.; Wales, D. J. *Chem. Phys. Lett.* **1986**, *128*, 501–503.

(68) Perdew, J. P.; Chevary, J. A.; Vosko, S. H.; Jackson, K. A.; Pederson, M. R.; Singh, D. J.; Fiolhais, C. *Phys. Rev. B* **1992**, *46*, 6671–6687.

(69) Kresse, G.; Hafner, J. *Phys. Rev. B* **1993**, *47*, 558–561.

(70) Kresse, G.; Hafner, J. *Phys. Rev. B* **1994**, *49*, 14251–14269.

(71) Kresse, G.; Furthmuller, J. *Comput. Mater. Sci.* **1996**, *6*, 15–50.

(72) Kresse, G.; Furthmuller, J. *Phys. Rev. B* **1996**, *54*, 11169–11186.

(73) Vanderbilt, D. *Phys. Rev. B* **1990**, *41*, 7892–7895.

(74) Haddon, R. C. *J. Am. Chem. Soc.* **1986**, *108*, 2837–2842.

(75) Haddon, R. C. *J. Am. Chem. Soc.* **1987**, *109*, 1676–1685.

(76) Haddon, R. C. *J. Am. Chem. Soc.* **1990**, *112*, 3385–3389.

(77) Yang, S. H.; Shin, W. H.; Kang, J. K. *J. Chem. Phys.* **2006**, *125*, 084705.

(78) Pan, B. C.; Yang, W. S.; Yang, J. L. *Phys. Rev. B* **2000**, *62*, 12652–12655.

(79) Horner, D. A.; Redfern, P. C.; Sternberg, M.; Zapol, P.; Curtiss, L. A. *Chem. Phys. Lett.* **2007**, *450*, 71–75.

(80) Ouyang, F. P.; Huang, B.; Li, Z.; Xiao, J.; Wang, H.; Xu, H. *J. Phys. Chem. C* **2008**, *112*, 12003–12007.